Engineering and Applied Science Letters

PSR Press

*Article*

# Hall current and chemical reaction effects on MHD partial-slip Ferrofluid flow over a permeable stretching sheet

**Khaled K. Jaber**

Department of Mathematics, Faculty of Science, Isra University, Amman, Jordan; khaled.jaber@iu.edu.jo.

Received: 21 March 2026; Accepted: 05 June 2026; Published: 22 June 2026.

**Abstract:** The steady magnetohydrodynamic boundary-layer flow of a conducting ferro-nanofluid over a permeable stretching sheet of variable thickness subject to Hall effect, thermal radiation, viscous dissipation, Brownian diffusion, thermophoresis and first order chemical reaction is analyzed. A uniform transverse magnetic field along with the consideration of the Hall effect produces an additional secondary fluid motion in association with the main stretching flow. Applying the similarity transformation technique, the governing equations of conservation of mass, momentum, energy and species concentrations are transformed into a nonlinear system of ordinary differential equations. The numerical solution of the similarity equation with proper boundary conditions is obtained using a fourth order Runge-Kutta shooting algorithm under appropriate convergence criteria. It is found that a higher magnetic parameter decreases the main flow velocity and increases the secondary velocity due to Hall effect. Thermal boundary layer thickness increases with increasing Brownian motion and thermophoresis but decreases with increasing chemical reaction rate and Lewis number. The wall gradient profiles reveal that an increase in the interaction between magnetic field and flow leads to enhance the magnitude of the primary shear as well as significantly changes the heat and mass transfer.

**Keywords:** Hall current, magnetohydrodynamics, ferrofluid, stretching sheet, thermal radiation, chemical reaction, nanoparticle transport

## 1. Introduction

Boundary-layer flow induced by a stretching sheet is a basic model that describes heat and mass transport in applications ranging from extrusion and manufacturing of polymer sheets to wire drawing, cooling of metallic sheets, coating operations and microfluidic devices. The stretching velocity regulates the wall shear stress, the thickness of the thermal boundary layer and the rate of removal of mass from the wall. Initial work on the influence of wall suction or blowing on heat and mass transfer in stretching sheets can be traced back to [1]. Subsequent investigations involved generalized stretching and shrinking walls with convective heating [2] and unsteady permeable stretching sheets with non-uniform heat generation or absorption [3]. Thus, small variations in the wall movement and boundary conditions produce a great impact on transport phenomena.

Models involving non-Newtonian and complicated fluids have been employed to describe physiological, polymeric and industrial fluids in boundary-layer configurations. Fluids of Jeffrey type were used to study peristaltic flow, magnetically affected motion in channels and stagnation flow near stretching/shrinking walls [4–8]. Concurrently, magnetohydrodynamic (MHD) models have gained considerable importance owing to the fact that the application of magnetic field gives a means for regulation of the electrically conducting fluid without any contact. Stagnation-point MHD flow, dusty fluid stagnation-layer flow and viscoelastic channel flow were studied under various assumptions about magnetic and thermal fields [9–11]. These works form the basis of controlling the velocity field by means of Lorentz forces.

Nanofluids serve as an additional tool for thermal management because the suspension of nanoparticles results in the modification of thermal conductivity and microscale heat and mass transport. The idea of enhancing thermal conductivity of the base fluid by the addition of nanoparticles has been put forward by Choi [12]. Since then, analytical and numerical approaches have been developed in order to examine MHD

convection of nanofluid, thermodiffusion, entropy generation, temperature-dependent viscosity and buoyancy effects in flows past stretching sheets [13–17]. The Brownian motion and thermophoresis effects are particularly important for these problems because they link the energy and mass transfer equations. In this context, the papers devoted to transport of nanoparticles in channels and magnetohydrodynamic nanofluid flows also suggest that viscous dissipation and variations of the material properties affect the heat transfer at the wall significantly [18–21].

Radiation plays an important role in problems involving manufacturing processes at elevated temperatures, solar thermal applications, nuclear engineering and metallurgical processes. There exists a number of works on the MHD boundary layer flows induced by stretching sheets with account for thermally stratified medium, two-phase nanofluid model and effects of buoyancy [22–24]. If the temperature difference is sufficiently large, radiative heat flux affects the diffusion of thermal energy and makes the neglect of radiation effects rather crude approximation. Effects of variation of viscosity, thermophoresis and radiation have been accounted for in the problem of MHD flow in a porous medium over a heated wall [25], while radiation heat generation/absorption was examined in the case of viscoelastic stretching-sheet flow [26].

Partial slip, porous drag, Hall current and chemical reaction are other physical effects that should be taken into account when one deals with small-scale devices, rarefied or micro-scale flows, reactive coating and electrically conducting suspension. Works on the partial slip effects in rotating channels, micropolar fluids and magnetite nanoparticle flow show that the interaction between the fluid and wall may affect both the momentum and heat transfer [27–29]. Thermodiffusion and diffusion-thermo effects in nanofluid boundary layers were also studied in [30], and variable property nanofluid flow over a permeable stretching sheet with radiation and viscous dissipation was considered in [31].

The present analysis deals with the influence of Hall current and chemical reaction on MHD ferro-nanofluid flow over a permeable stretching sheet of variable thickness. Its distinctive feature lies in the fact that Hall current, porous drag, variation of surface geometry, radiation, viscous dissipation, Brownian diffusion and thermophoresis effects are taken into account simultaneously. This coupling is important because each of these effects has a specific role in the process of transport - the Hall term redistributes momentum in the primary and secondary directions, while radiation and viscous dissipation affect the temperature field and chemical reaction modifies the mass transfer.

## 2. Mathematical formulation

The physical setting is shown in Figure 1. A steady, laminar, incompressible ferro-nanofluid flows over a stretching sheet whose surface is described by

$$y = A(x+b)^{\frac{1-n}{2}}, \quad A > 0, \quad b > 0. \tag{1}$$

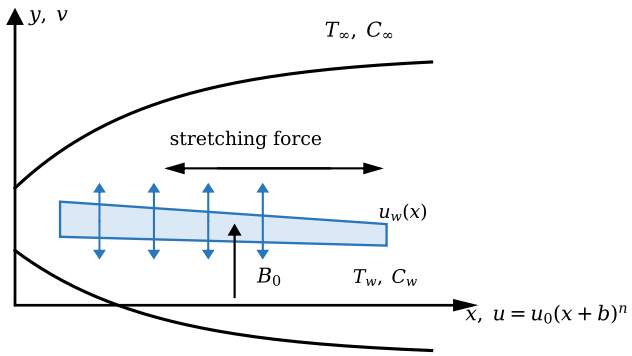


**Figure 1.** Physical configuration and coordinate system for the permeable variable-thickness stretching sheet

The stretching velocity is chosen as $u_w(x) = u_0(x+b)^n$ with $u_0 > 0$ and $n$ being the power-law index. Permeability of the sheet is allowed, and suction/injection is described by the wall velocity $v_w(x)$ in the normal

direction. The temperature at the wall and ambient is $T_w$ and $T_\infty$, and similarly the concentration at the wall and ambient is $C_w$ and $C_\infty$.

A constant magnetic field $B_0$ is applied perpendicular to the plate. The value of the magnetic Reynolds number is considered small, hence, the induced magnetic field is ignored. The Hall effect is accounted for in the equation of Ohm's law, and as a result, another velocity component called $w$ is generated along with the velocity components $u$ and $v$. The differential equations are

$$\frac{\partial u}{\partial x}+\frac{\partial v}{\partial y}=0, \tag{2}$$

$$\rho_{nf}\left(u\frac{\partial u}{\partial x}+v\frac{\partial u}{\partial y}\right)=\mu_{nf}\frac{\partial^2 u}{\partial y^2}-\frac{\sigma B_0^2}{1+m^2}(u+mw)-\frac{\mu_{nf}}{K'}u, \tag{3}$$

$$\rho_{nf}\left(u\frac{\partial w}{\partial x}+v\frac{\partial w}{\partial y}\right)=\mu_{nf}\frac{\partial^2 w}{\partial y^2}-\frac{\sigma B_0^2}{1+m^2}(mu-w)-\frac{\mu_{nf}}{K'}w, \tag{4}$$

$$(\rho C_p)_{nf}\left(u\frac{\partial T}{\partial x}+v\frac{\partial T}{\partial y}\right)=k_{nf}\frac{\partial^2 T}{\partial y^2}+(\rho C_p)_p\left\{D_B\frac{\partial C}{\partial y}\frac{\partial T}{\partial y}+\frac{D_T}{T_\infty}\left(\frac{\partial T}{\partial y}\right)^2\right\}+\mu_{nf}\left(\frac{\partial u}{\partial y}\right)^2-\frac{\partial q_r}{\partial y}, \tag{5}$$

$$u\frac{\partial C}{\partial x}+v\frac{\partial C}{\partial y}=D_B\frac{\partial^2 C}{\partial y^2}+\frac{D_T}{T_\infty}\frac{\partial^2 T}{\partial y^2}-k_c(C-C_\infty). \tag{6}$$

The corresponding boundary conditions are written as

$$\begin{cases} u=u_w(x)+u_s(x), \quad v=v_w(x), \quad w=0, \quad T=T_w, \quad C=C_w, \quad y=A(x+b)^{\frac{1-n}{2}}, \\ u\to 0, \quad w\to 0, \quad T\to T_\infty, \quad C\to C_\infty, \quad y\to\infty. \end{cases} \tag{7}$$

The term $u_s(x)$ represents the slip contribution to the tangential wall velocity. The Brownian diffusion coefficient is

$$D_B=\frac{k_B T C}{3\pi\mu d_p}, \tag{8}$$

where $k_B$ is Boltzmann's constant and $d_p$ is the nanoparticle diameter.

The Rosseland diffusion approximation is used for the radiative heat flux,

$$q_r=-\frac{4\sigma^*}{3K^*}\frac{\partial T^4}{\partial y}, \tag{9}$$

where $K^*$ is the mean absorption coefficient. Expanding $T^4$ about $T_\infty$ and neglecting higher-order terms gives

$$T^4\simeq 4T_\infty^3 T-3T_\infty^4. \tag{10}$$

The boundary condition imposed at the variable-thickness surface is mapped to $\eta=0$ by introducing

$$\eta=\sqrt{\frac{u_0(n+1)}{2\nu_f}}\,(x+b)^{\frac{n-1}{2}}y-A\sqrt{\frac{u_0(n+1)}{2\nu_f}}, \tag{11}$$

and the dimensionless variables

$$\psi=\sqrt{\frac{2\nu_f u_0}{n+1}}\,(x+b)^{\frac{n+1}{2}}f(\eta), \quad w=u_w(x)h(\eta), \quad \theta(\eta)=\frac{T-T_\infty}{T_w-T_\infty}, \quad \phi(\eta)=\frac{C-C_\infty}{C_w-C_\infty}. \tag{12}$$

The stream function satisfies $u=\partial\psi/\partial y$ and $v=-\partial\psi/\partial x$, and therefore

$$u=u_w f'(\eta), \quad v=-\sqrt{\frac{(n+1)\nu_f u_w}{2(x+b)}}\left[f(\eta)+\frac{n-1}{n+1}\eta f'(\eta)\right]. \tag{13}$$

Here and throughout, a prime denotes differentiation with respect to $\eta$.

Using Eqs. (11)–(13), the governing equations reduce to

$$f''' = \frac{\rho_1}{\mu_1}\left(\frac{2n}{n+1}f'^2 - ff''\right) + \frac{2M}{\mu_1(n+1)(1+m^2)}(f' + mh) + \frac{2K_p}{n+1}f', \tag{14}$$

$$h'' = \frac{\rho_1}{\mu_1}\left(\frac{2n}{n+1}hf' - fh'\right) - \frac{2M}{\mu_1(n+1)(1+m^2)}(mf' - h) - \frac{2K_p}{n+1}h, \tag{15}$$

$$\theta'' + \frac{Pr}{\tau K_1}\left[f\theta' + N_b\theta'\phi' + N_t\theta'^2 + 4R\tau\theta'' + Ec\tau\mu_1 f''^2\right] = 0, \tag{16}$$

$$\phi'' + \frac{N_t}{N_b}\theta'' + Le\, f\phi' - K_r\phi = 0. \tag{17}$$

The dimensionless parameters are

$$\begin{cases} M = \frac{\sigma B_0^2(x+b)}{\rho_f u_w}, \quad K_p = \frac{2\nu_f(x+b)}{K' u_w}, \quad Pr = \frac{\mu_f(C_p)_f}{k_f}, \quad Ec = \frac{u_w^2}{(C_p)_f(T_w - T_\infty)}, \\ Le = \frac{\nu_f}{D_B}, \quad N_b = \frac{(\rho C_p)_p D_B(C_w - C_\infty)}{(\rho C_p)_{nf}\nu_f}, \quad N_t = \frac{(\rho C_p)_p D_T(T_w - T_\infty)}{(\rho C_p)_{nf} T_\infty \nu_f}, \\ K_r = \frac{k_c(x+b)}{u_w}, \quad R = \frac{4\sigma^* T_\infty^3}{3k^* k_f}, \quad K_1 = \frac{k_{nf}}{k_f}, \quad \mu_1 = \frac{\mu_{nf}}{\mu_f}, \quad \rho_1 = \frac{\rho_{nf}}{\rho_f}. \end{cases}$$

The transformed boundary conditions are

$$\begin{cases} f(0) = S, \quad f'(0) = 1, \quad h(0) = 0, \quad \theta(0) = 1, \quad \phi(0) = 1, \\ f'(\eta) \to 0, \quad h(\eta) \to 0, \quad \theta(\eta) \to 0, \quad \phi(\eta) \to 0, \quad \eta \to \infty, \end{cases} \tag{18}$$

where the suction/injection parameter is

$$S = -\frac{v_w}{\nu_f}\left[\frac{(n+1)(x+b)^{n-1}}{2}\right]^{-1/2}. \tag{19}$$

The wall gradients determine the engineering quantities of interest. With

$$\tau_{w1} = -\mu_{nf}\left.\frac{\partial u}{\partial y}\right|_w, \quad \tau_{w2} = -\mu_{nf}\left.\frac{\partial w}{\partial y}\right|_w, \quad q_w = -k_{nf}\left.\frac{\partial T}{\partial y}\right|_w, \quad q_m = -D_B\left.\frac{\partial C}{\partial y}\right|_w, \tag{20}$$

the local skin-friction coefficients, Nusselt number and Sherwood number are

$$C_{fx} = \frac{2\tau_{w1}}{\rho_f u_w^2}, \quad C_{fz} = \frac{\tau_{w2}}{\rho_f u_w^2}, \quad Nu_x = \frac{(x+b)q_w}{k_f(T_w - T_\infty)}, \quad Sh_x = \frac{(x+b)q_m}{D_B(C_w - C_\infty)}. \tag{21}$$

The reduced forms are

$$Re_x^{1/2} C_{fx} = \mu_1\sqrt{2(n+1)}\, f''(0), \tag{22}$$

$$Re_x^{1/2} C_{fz} = \mu_1\sqrt{\frac{n+1}{2}}\, h'(0), \tag{23}$$

$$Re_x^{-1/2} Nu_x = -K_1\sqrt{\frac{n+1}{2}}\, \theta'(0), \tag{24}$$

$$Re_x^{-1/2} Sh_x = -\sqrt{\frac{n+1}{2}}\, \phi'(0), \tag{25}$$

where $Re_x = u_w(x+b)/\nu_f$.

## 3. Numerical solution

The coupled equations (14)–(17), with the boundary conditions (18) applied, were solved numerically via a fourth-order Runge-Kutta shooting method. The initial slopes of the unknown functions were iteratively modified until the far-field values of $f'$, $h$, $\theta$ and $\phi$ were met on a finite domain. This finite domain was made

to be increasingly large, such that no more significant difference was seen in the profiles or the wall gradients when further increasing its size. The stopping criteria for the solution process was:

$$\max_j \left| Y_j^{(r+1)} - Y_j^{(r)} \right| < 10^{-9}, \tag{26}$$

where $Y_j$ denotes the shooting variables at iteration $r$. Unless otherwise stated, the reference values used in the parametric study are $Pr = 0.72$, $R = 0.1$, $\tau = 1$, $N_b = 0.2$, $N_t = 0.1$, $K_r = 0.1$, $Le = 0.1$, $Ec = 0.1$, $K_1 = 1$, $\mu_1 = 1$, $\rho_1 = 0.1$, $m = 1$ and $M = 0.2$.

## 4. Results and discussion

The results are given in terms of dimensionless temperature $\theta$, concentration $\phi$, primary flow $f'$ and induced Hall effect $h$. All graphs and values of gradients are expressed using the notation similar to Eqs. (14)–(17), making it possible to directly compare the influence of momentum interaction, heat transport and mass transfer on the boundary layer.

The influence of Brownian diffusion on the thermal boundary layer is illustrated in Fig. 2. With an increase in $N_b$, the value of $\theta$ increases within the whole thickness of the thermal boundary layer. From a physical point of view, this means that an increased Brownian diffusion causes higher nanoparticle agitations and leads to the increase of energy exchange at the micrometer scale between nanoparticles and the base fluid. As a result, the thickness of the thermal boundary layer increases, and the rate of temperature fall decreases.

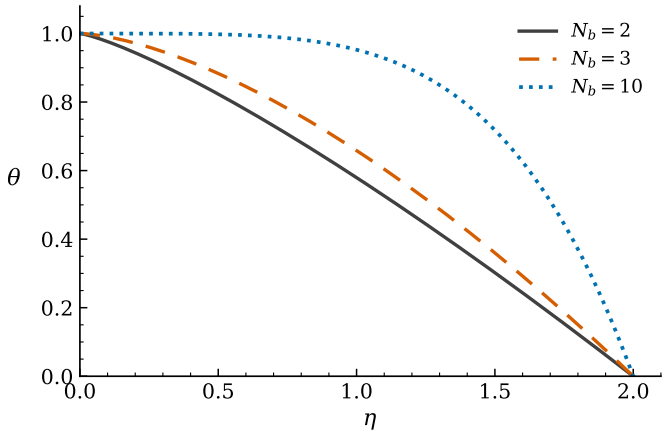


**Figure 2.** Influence of Brownian motion parameter $N_b$ on the temperature profile

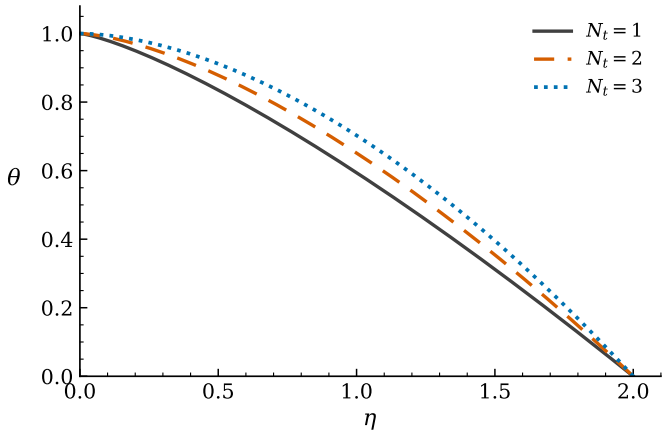


**Figure 3.** Influence of thermophoresis parameter $N_t$ on the temperature profile

The influence of thermophoresis on temperature distribution is shown in Figure 3. Higher values of $N_t$ lead to increased temperature distribution due to the movement of nanoparticles from hot zones close to the

wall into cooler zones of the outer boundary layer. The influence is lower compared to the one with a high value of $N_b$, but still monotonic for the interval considered.

The distribution of nanoparticle concentration reacts to thermophoresis in a different way, as shown in Figure 4. Increasing $N_t$ leads to a decrease in $\phi$. The reason for this phenomenon lies in the fact that even though thermophoresis intensifies the energy transfer process, it also results in the movement of particles from the hot wall region to cooler ones. Thus, we can conclude that both temperature and concentration boundary layers do not necessarily respond similarly to the movement of nanoparticles. When analyzing both figures, i.e., Fig. 3 and Fig. 4, it is evident that thermal and concentration boundary layers do not have to react in the same way towards nanoparticle movement.

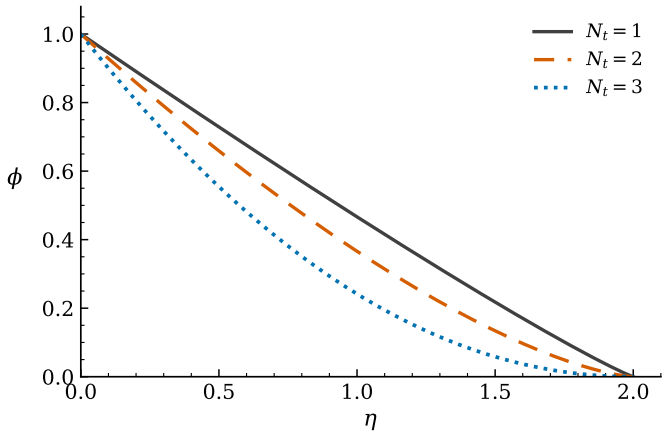


**Figure 4.** Influence of thermophoresis parameter $N_t$ on the concentration profile

This is described by Figs. 5 and 6. As $K_1$ becomes higher, there is a growth in the concentration profile and a decrease in the temperature profile. There is a lower thermal field because the increased thermal conductivity causes an increase in the rate of heat transfer in the wall, thereby bringing the temperature close to the ambient temperature quickly. The growth in the concentration field occurs as a result of the change in the thermal diffusion effect leading to a shift in the ratio between the Brownian and the thermophoretic transport in the concentration equation. The coupled nature of Eqs. (16) and (17) is clearly evident here since thermal conductivity influences both energy and species transport.

There is an effect of chemical reaction on concentration since it dampens it as shown in Fig. 7. The term $-K_r\phi$ in Eq. (17) acts as the consumption of the species in the concentration boundary layer. Thus, as $K_r$ is made higher, there is a sharper decline in $\phi$. Such a behavior is also in accordance with reactive coating and catalytic surface reactions, where higher rates of reaction decrease the concentration at the wall.

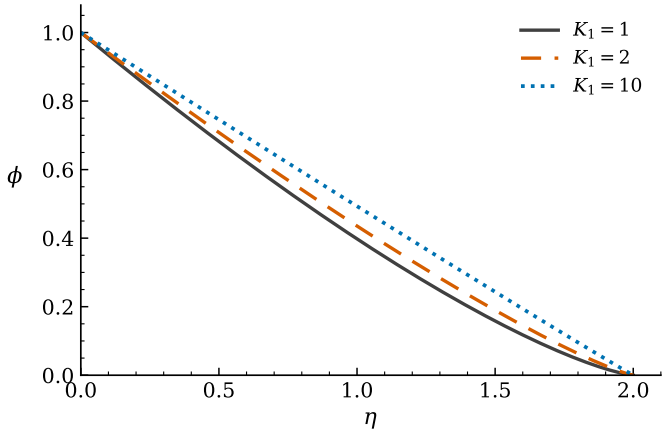


**Figure 5.** Influence of thermal-conductivity ratio $K_1$ on the concentration profile

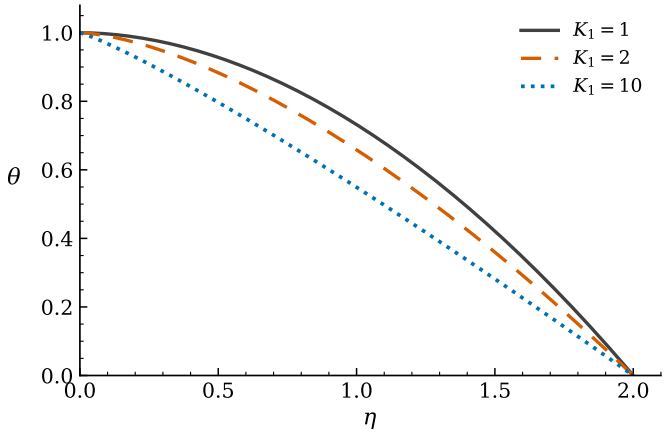


**Figure 6.** Influence of thermal-conductivity ratio $K_1$ on the temperature profile

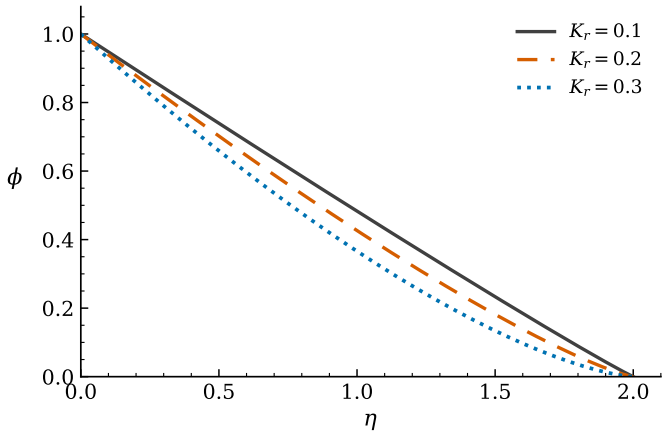


**Figure 7.** Influence of chemical reaction parameter $K_r$ on the concentration profile

The influence of the magnetic parameter on the two velocity components is of an opposing nature. While the secondary velocity in Fig. 8 rises with increase of $M$, the primary velocity in Fig. 9 falls. The primary flow experiences retarding effect due to the Lorentz force that serves as an electromagnetic resistance in the direction of stretching. However, the action of the Hall current changes the picture so that some of the electromagnetic forcing is transferred to the secondary flow.

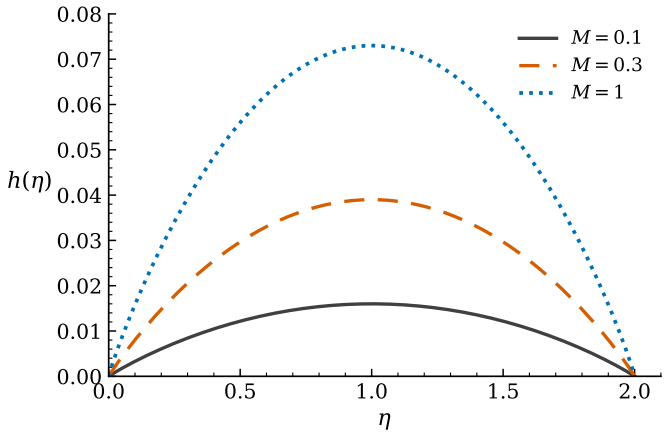


**Figure 8.** Influence of magnetic parameter $M$ on the Hall-induced secondary velocity $h$

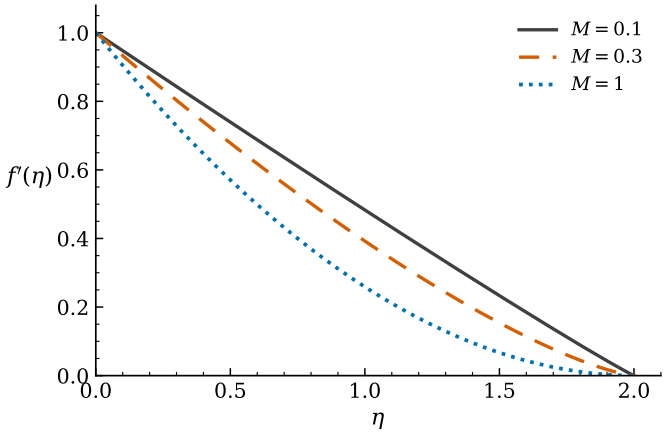


**Figure 9.** Influence of magnetic parameter $M$ on the primary velocity $f'$

The density ratio affects the secondary flow via its effect on the inertial part of Eq. (15). Figure 10 shows that the increase of $\rho_1$ results in weakening $h$. As the effective density is increased, the inertial part dominates over the viscous diffusion and magnetic parts, and thus the secondary flow generated by the Hall term is reduced. The above observation becomes critical when comparing ferrofluids with different nanoparticle loadings since an increase in the loading will improve thermal performance but reduce secondary flow.

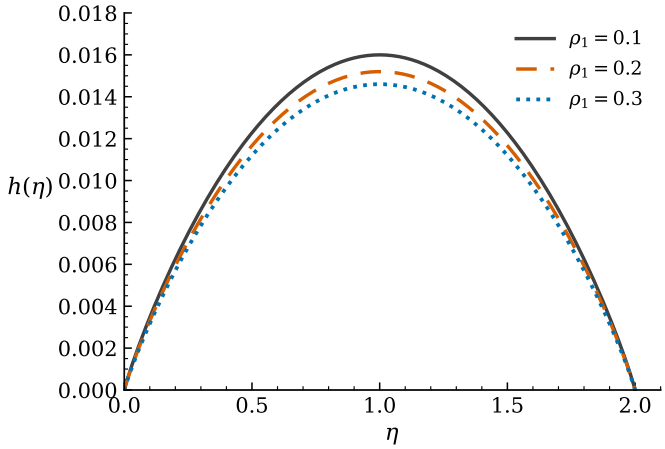


**Figure 10.** Influence of density ratio $\rho_1$ on the secondary velocity $h$

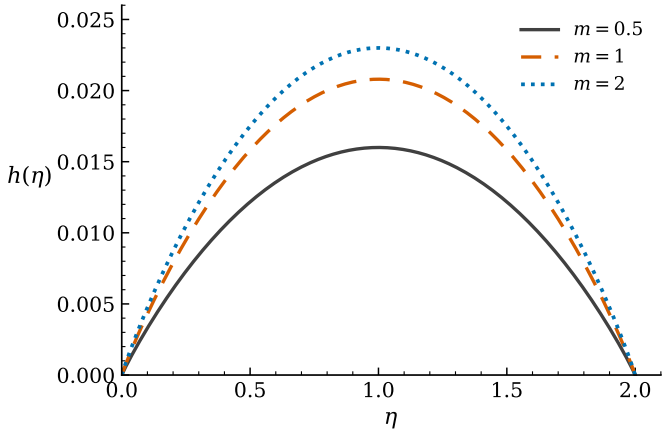


**Figure 11.** Influence of Hall parameter $m$ on the secondary velocity $h$

An increase in the value of Hall parameter leads to an increase in the secondary velocity as demonstrated by Figure 11. Hall effect weakens the entirely resistive nature of the Lorentz force in the primary flow direction and couples momentum equation through $u$ and $w$. With the increase in the Hall parameter, $m$, the effect strengthens the transverse flow and widens the range for which $h$ is greater than zero. The analysis reveals that Hall current plays a significant role and not just a secondary effect on the flow characteristics as it dictates the secondary velocity magnitude.

The power-law exponent governs the variation in the stretching velocity. Figure 12 indicates that increasing the value of the power-law index results in a decrease in the secondary velocity. With increasing values of $n$, the longitudinal stretching variation and hence convective effect in the transformed momentum equations become stronger. This modifies the balance between the magnetic effect on secondary motions and viscous diffusion, causing a reduction in the transverse velocity field.

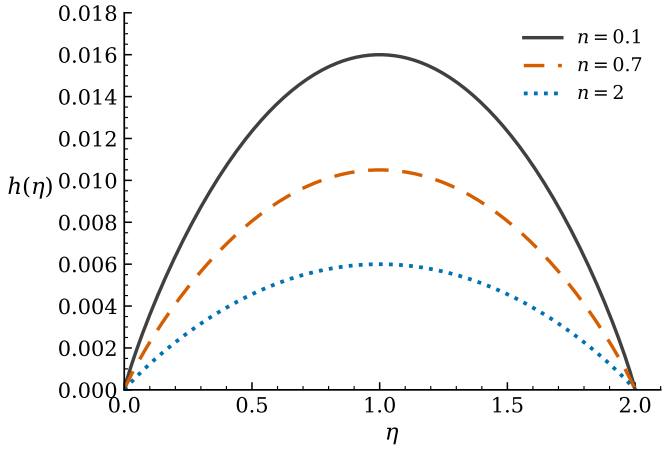


**Figure 12.** Influence of stretching power-law index $n$ on the secondary velocity $h$

An increase in the Lewis number causes a decrease in the concentration profile as illustrated in Figure 13. With the definition of Lewis number $Le = \nu_f / D_B$, higher values of $Le$ imply weaker Brownian mass transport compared to the momentum transfer. Hence, the species boundary layer becomes smaller and the concentration tends to be equal to the ambient concentration faster. The trend can be attributed to the decrease in concentration due to chemical reaction, but the mechanism works differently since large values of $Le$ decrease diffusive transport, while large values of $K_r$ remove the species through reactions.

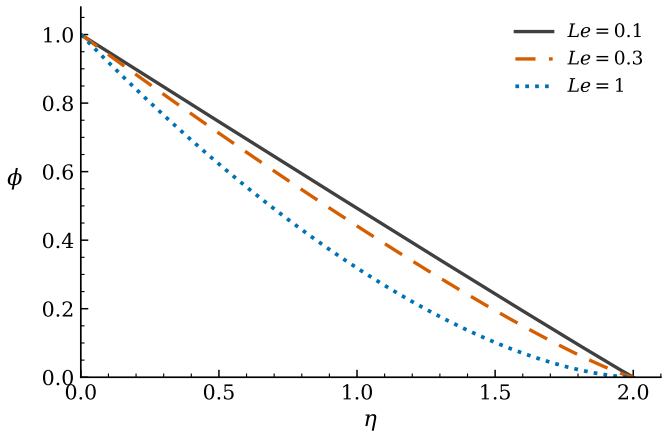


**Figure 13.** Influence of Lewis number $Le$ on the concentration profile

The radiation parameter impacts the thermal and concentration distributions in opposite manners. From Figure 14, one can conclude that the increase in the radiation parameter leads to a decrease in the temperature distribution. Increased radiative diffusion promotes the extraction of thermal energy from the near-wall region and makes the temperature of the fluid approach the ambient temperature faster. On the other hand,

the increase in the radiation parameter causes an increase in the concentration distribution illustrated in Figure 15. The two profiles therefore demonstrate the indirect coupling between radiation and nanoparticle concentration.

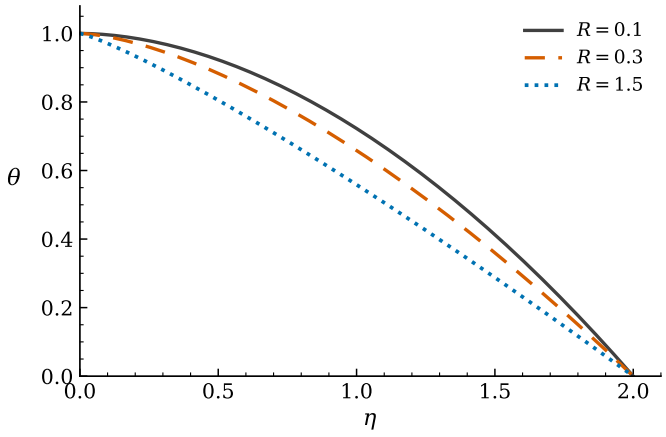


**Figure 14.** Influence of radiation parameter $R$ on the temperature profile

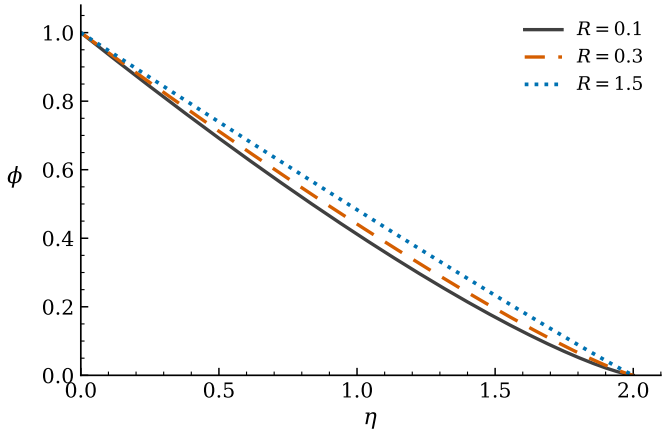


**Figure 15.** Influence of radiation parameter $R$ on the concentration profile

**Table 1.** Effects of selected parameters on wall gradients with $N_b = n = 0.2$, $N_t = K_r = R = Ec = Le = 0.1$ and $K_1 = \mu_1 = \tau = 1$ unless varied

| $K_r$ | $K_1$ | $\rho_1$ | $m$ | $M$ | $-f''(0)$ | $h'(0)$ | $-\theta'(0)$ | $-\phi'(0)$ |
|---|---|---|---|---|---|---|---|---|
| 0.1 | 1 | 0.1 | 0.5 | 0.2 | 0.729739 | 0.044276 | 0.252135 | 0.694323 |
| 0.2 | 1 | 0.1 | 0.5 | 0.2 | 0.729739 | 0.044276 | 0.256174 | 0.721444 |
| 0.3 | 1 | 0.1 | 0.5 | 0.2 | 0.729739 | 0.044276 | 0.263518 | 0.729462 |
| 0.1 | 2 | 0.1 | 0.5 | 0.2 | 0.729739 | 0.044276 | 0.344292 | 0.651537 |
| 0.1 | 10 | 0.1 | 0.5 | 0.2 | 0.729739 | 0.044276 | 0.461247 | 0.598659 |
| 0.1 | 1 | 0.2 | 0.5 | 0.2 | 0.756939 | 0.043459 | 0.250457 | 0.694861 |
| 0.1 | 1 | 0.3 | 0.5 | 0.2 | 0.783614 | 0.042673 | 0.248818 | 0.695387 |
| 0.1 | 1 | 0.1 | 1.0 | 0.2 | 0.699617 | 0.056812 | 0.253448 | 0.693928 |
| 0.1 | 1 | 0.1 | 2.0 | 0.2 | 0.667911 | 0.046717 | 0.254844 | 0.693507 |
| 0.1 | 1 | 0.1 | 0.5 | 1.0 | 1.111080 | 0.373268 | 0.543970 | 0.554368 |
| 0.1 | 1 | 0.1 | 0.5 | 2.0 | 1.489120 | 0.573099 | 0.519111 | 0.562586 |

The information about the wall gradients presented in Table 1 complements the profile behavior observations. As can be seen from Table 1, an increase of $K_r$ does not influence the momentum wall gradients as the reaction term occurs only in the concentration equation, but it leads to an increase in the magnitudes

of $-\theta'(0)$ and $-\phi'(0)$ due to the coupled thermal and species equations. The reduction in the concentration profile with $K_r$ is therefore followed by an increase in the concentration wall gradient. An increase in the wall thermal gradient and the reduction of the concentration wall gradient with increase of $K_1$ indicate that an improvement in the thermal conduction and species diffusion processes does not necessarily mean the simultaneous change of the corresponding coefficients. The wall primary shear increases with increase in $\rho_1$, and the wall secondary shear is slightly reduced, while changes in the Hall parameter affect mostly the wall shear distribution. Finally, the magnetic parameter causes the most significant changes of the wall shears: the magnitudes of $-f''(0)$ and $h'(0)$ increase significantly with an increase of $M$ that is in agreement with the profile observations demonstrating the suppression of the primary velocity by magnetic forcing and enhancement of the secondary velocity.

## 5. Conclusion

This paper analyzed the effects of Hall current and chemical reaction on MHD ferro-nanofluid flow over a permeable stretched sheet of variable thickness under the action of radiation, viscous dissipation, Brownian motion and thermophoresis.

It was shown that electromagnetic forcing has a dual effect on the momentum transport. The increase in the magnetic parameter leads to the suppression of the primary velocity due to the action of Lorentz drag but enhances the Hall current-induced secondary velocity due to the cross-flow coupling. In turn, the increase in the Hall parameter strengthens the secondary flow and changes the components of wall shear. Heat transfer process is enhanced by the actions of Brownian motion and thermophoresis leading to thickening of the thermal boundary layer, and the thermal conductivity ratio and radiation accelerate the rate of temperature decay in the thermal boundary layer. Species transport is reduced by the effect of chemical reaction and by the increase of the Lewis number which cause the reduction in the concentration boundary layer.

As one can see from the wall-gradient information, the behavior of profiles cannot be explained simply by the change of boundary-layer thickness. Thus, an increase of the wall concentration gradient occurs due to chemical reaction despite decreasing the concentration field; increase of the thermal gradient with the reduction of the concentration gradient is observed with increasing thermal conductivity; and the wall shear is increased significantly by magnetic forcing. Therefore, the consideration of Hall current, nanoparticle transport and chemical reaction in predicting the flow characteristics becomes important for electrically conducting ferrofluid flows over permeable stretching surfaces.

**Acknowledgments:** The author thanks Isra University for academic support.

**Conflicts of Interest:** The author declares no conflict of interest.

### References

[1] Gupta, P. S., & Gupta, A. S. (1977). Heat and mass transfer on a stretching sheet with suction or blowing. *The Canadian Journal of Chemical Engineering, 55*(6), 744-746.

[2] Yao, S., Fang, T., & Zhong, Y. (2011). Heat transfer of a generalized stretching/shrinking wall problem with convective boundary conditions. *Communications in Nonlinear Science and Numerical Simulation, 16*(2), 752-760.

[3] Zheng, L., Wang, L., & Zhang, X. (2011). Analytic solutions of unsteady boundary flow and heat transfer on a permeable stretching sheet with non-uniform heat source/sink. *Communications in Nonlinear Science and Numerical Simulation, 16*(2), 731-740.

[4] Vajravelu, K., Sreenadh, S., & Lakshminarayana, P. (2011). The influence of heat transfer on peristaltic transport of a Jeffrey fluid in a vertical porous stratum. *Communications in Nonlinear Science and Numerical Simulation, 16*(8), 3107-3125.

[5] Kothandapani, M., & Srinivas, S. (2008). Peristaltic transport of a Jeffrey fluid under the effect of magnetic field in an asymmetric channel. *International Journal of Non-Linear Mechanics, 43*(9), 915-924.

[6] Pandey, S. K., & Tripathi, D. (2010). Unsteady model of transportation of Jeffrey-fluid by peristalsis. *International Journal of Biomathematics, 3*(04), 473-491.

[7] Dalir, N. (2014). Numerical study of entropy generation for forced convection flow and heat transfer of a Jeffrey fluid over a stretching sheet. *Alexandria Engineering Journal, 53*(4), 769-778.

[8] Turkyilmazoglu, M., & Pop, I. (2013). Exact analytical solutions for the flow and heat transfer near the stagnation point on a stretching/shrinking sheet in a Jeffrey fluid. *International Journal of Heat and Mass Transfer, 57*(1), 82-88.

[9] Ali, F. M., Nazar, R., Arifin, N. M., & Pop, I. (2011). MHD stagnation-point flow and heat transfer towards stretching sheet with induced magnetic field. *Applied Mathematics and Mechanics, 32*(4), 409-418.

[10] Ramesh, G. K., Gireesha, B. J., & Bagewadi, C. S. (2012). MHD flow of a dusty fluid near the stagnation point over a permeable stretching sheet with non-uniform source/sink. *International Journal of Heat and Mass Transfer, 55*(17-18), 4900-4907.

[11] Raftari, B., & Vajravelu, K. (2012). Homotopy analysis method for MHD viscoelastic fluid flow and heat transfer in a channel with a stretching wall. *Communications in Nonlinear Science and Numerical Simulation, 17*(11), 4149-4162.

[12] Choi, S. U. (1995, November). Enhancing thermal conductivity of fluids with nanoparticles. In *Asme International Mechanical Engineering Congress and Exposition* (Vol. 17421, pp. 99-105). American Society of Mechanical Engineers.

[13] Hamad, M. A. A. (2011). Analytical solution of natural convection flow of a nanofluid over a linearly stretching sheet in the presence of magnetic field. *International Communications in Heat and Mass Transfer, 38*(4), 487-492.

[14] Khan, U., Ahmed, N., Khan, S. I. U., & Mohyud-din, S. T. (2014). Thermo-diffusion effects on MHD stagnation point flow towards a stretching sheet in a nanofluid. *Propulsion and Power Research, 3*(3), 151-158.

[15] Rana, P., & Bhargava, R. (2012). Flow and heat transfer of a nanofluid over a nonlinearly stretching sheet: a numerical study. *Communications in Nonlinear Science and Numerical Simulation, 17*(1), 212-226.

[16] Govindaraju, M., Ganesh, N. V., Ganga, B., & Abdul Hakeem, A. K. (2015). Entropy generation analysis of magneto hydrodynamic flow of a nanofluid over a stretching sheet. *Journal of the Egyptian Mathematical Society, 23*(2), 429-434.

[17] Akbar, N. S., Tripathi, D., Khan, Z. H., & Bég, O. A. (2016). A numerical study of magnetohydrodynamic transport of nanofluids over a vertical stretching sheet with exponential temperature-dependent viscosity and buoyancy effects. *Chemical Physics Letters, 661*, 20-30.

[18] Sheikholeslami, M., Gorji-Bandpy, M., & Ganji, D. D. (2014). Lattice Boltzmann method for MHD natural convection heat transfer using nanofluid. *Powder Technology, 254*, 82-93.

[19] Sheikholeslami, M., & Ganji, D. D. (2015). Nanofluid flow and heat transfer between parallel plates considering Brownian motion using DTM. *Computer Methods in Applied Mechanics and Engineering, 283*, 651-663.

[20] Hayat, T., Khan, M. I., Waqas, M., Yasmeen, T., & Alsaedi, A. (2016). Viscous dissipation effect in flow of magnetonanofluid with variable properties. *Journal of Molecular Liquids, 222*, 47-54.

[21] Shehzad, S. A., Hussain, T., Hayat, T., Ramzan, M., & Alsaedi, A. (2015). Boundary layer flow of third grade nanofluid with Newtonian heating and viscous dissipation. *Journal of Central South University, 22*(1), 360-367.

[22] Mukhopadhyay, S. (2013). MHD boundary layer flow and heat transfer over an exponentially stretching sheet embedded in a thermally stratified medium. *Alexandria Engineering Journal, 52*(3), 259-265.

[23] Sheikholeslami, M., Ganji, D. D., Javed, M. Y., & Ellahi, R. (2015). Effect of thermal radiation on magnetohydrodynamics nanofluid flow and heat transfer by means of two phase model. *Journal of Magnetism and Magnetic Materials, 374*, 36-43.

[24] Rashidi, M. M., Ganesh, N. V., Hakeem, A. A., & Ganga, B. (2014). Buoyancy effect on MHD flow of nanofluid over a stretching sheet in the presence of thermal radiation. *Journal of Molecular Liquids, 198*, 234-238.

[25] Makinde, O. D., Khan, W. A., & Culham, J. R. (2016). MHD variable viscosity reacting flow over a convectively heated plate in a porous medium with thermophoresis and radiative heat transfer. *International Journal of Heat and Mass Transfer, 93*, 595-604.

[26] Cortell, R. (2014). MHD (magneto-hydrodynamic) flow and radiative nonlinear heat transfer of a viscoelastic fluid over a stretching sheet with heat generation/absorption. *Energy, 74*, 896-905.

[27] Raza, J., Rohni, A. M., Omar, Z., & Awais, M. (2016). Heat and mass transfer analysis of MHD nanofluid flow in a rotating channel with slip effects. *Journal of Molecular Liquids, 219*, 703-708.

[28] Ramzan, M., Farooq, M., Hayat, T., & Chung, J. D. (2016). Radiative and Joule heating effects in the MHD flow of a micropolar fluid with partial slip and convective boundary condition. *Journal of Molecular Liquids, 221*, 394-400.

[29] Hayat, T., Qayyum, S., Imtiaz, M., Alzahrani, F., & Alsaedi, A. (2016). Partial slip effect in flow of magnetite-$Fe_3O_4$ nanoparticles between rotating stretchable disks. *Journal of Magnetism and Magnetic Materials, 413*, 39–48.

[30] Jaber, K. K. (2023). Influence of Dofour and Soret on Eyrig-Powell Nanofluid Flow from A Circular Cylinder with Viscous Dissipation. *European Journal of Mathematics and Statistics, 4*(4), 69-77.

[31] Jaber, K. K. (2024). Variable fluid properties and partial slip effect of MHD flow of nanofluids over a permeable stretching sheet with heat radiation and viscous dissipation. *Jordan Journal of Mathematics and Statistics, 17*(3), 463-474.

## Nomenclature

| *Symbol* | *Meaning* | *Symbol* | *Meaning* |
|---|---|---|---|

| | | | |
|---|---|---|---|
| $A$ | thickness parameter of the sheet | $m$ | Hall current parameter |
| $b$ | positive shift parameter in the stretching law | $M$ | magnetic parameter |
| $B_0$ | applied magnetic-field strength | $n$ | power-law index of the stretching velocity |
| $C$ | nanoparticle concentration | $N_b$ | Brownian motion parameter |
| $C_p$ | specific heat at constant pressure | $N_t$ | thermophoresis parameter |
| $C_w, C_\infty$ | wall and ambient concentrations | $Nu_x$ | local Nusselt number |
| $D_B$ | Brownian diffusion coefficient | $Pr$ | Prandtl number |
| $D_T$ | thermophoretic diffusion coefficient | $q_m$ | wall mass flux |
| $Ec$ | Eckert number | $q_r$ | radiative heat flux |
| $f$ | dimensionless stream function | $q_w$ | wall heat flux |
| $h$ | dimensionless secondary velocity | $Re_x$ | local Reynolds number |
| $K'$ | porous-medium permeability | $R$ | radiation parameter |
| $K_1$ | thermal-conductivity ratio $k_{nf}/k_f$ | $S$ | suction/injection parameter |
| $K_p$ | porous-resistance parameter | $Sh_x$ | local Sherwood number |
| $K_r$ | chemical reaction parameter | $T$ | temperature |
| $k_c$ | dimensional reaction-rate coefficient | $T_w, T_\infty$ | wall and ambient temperatures |
| $Le$ | Lewis number | $u, v, w$ | velocity components in $x$, $y$ and transverse directions |
| *Greek symbols* | | | |
| $\eta$ | similarity variable | $\mu$ | dynamic viscosity |
| $\theta$ | dimensionless temperature | $\nu$ | kinematic viscosity |
| $\phi$ | dimensionless concentration | $\rho$ | density |
| $\sigma$ | electrical conductivity | $\sigma^*$ | Stefan-Boltzmann constant |
| $\tau$ | ratio of heat capacities | $\psi$ | stream function |
| *Subscripts* | | | |
| $f$ | base fluid | $nf$ | nanofluid or ferro-nanofluid |
| $w$ | wall condition | $\infty$ | ambient condition |